

Limits of Exciton-Exciton Annihilation for Light Emission in Transition Metal Dichalcogenide Monolayers

Yiling Yu^{1,2§}, Yifei Yu^{1§}, Chao Xu^{2§}, Andy Barrette², Kenan Gundogdu^{2*}, Linyou Cao^{1,2*}

¹Department of Materials Science and Engineering, North Carolina State University, Raleigh NC 27695; ²Department of Physics, North Carolina State University, Raleigh NC 27695;

§ These authors contribute equally.

Abstract

We quantitatively evaluate the exciton-exciton annihilation (EEA) and its effect on light emission properties in monolayer TMDC materials, including WS₂, MoS₂, and WSe₂. The EEA rate is found to be 0.3 cm²/s and 0.1 cm²/s for suspended WS₂ and MoS₂ monolayers, respectively, and subject to the influence from substrates, being 0.1 cm²/s and 0.05 cm²/s for the supported WS₂ and MoS₂ on sapphire substrates. It can substantially affect the luminescence efficiency of suspended monolayers even at an exciton concentration as low as 10⁹ cm⁻², but plays a milder role for supported monolayers due to the effect of the substrate. However, regardless the presence of substrates or not, the lasing threshold of the monolayer is always predominantly determined by the EEA, which is estimated to be 12-18 MW/cm² if using 532 nm as the pumping wavelength.

* To whom correspondence should be addressed

Email: lcao2@ncsu.edu, kgundog@ncsu.edu

Two-dimensional (2D) transition metal dichalcogenide (TMDC) materials such as monolayer MoS₂, WS₂, and WSe₂ promise to enable the development of atomic-scale light emission devices owing to perfect surface passivation and strong exciton binding energy [1]. A key to implementing the device development is to understand the exotic exciton dynamics of these materials. In particular, the extraordinary exciton binding energy [2-5], which may be one order of magnitude higher than that of conventional semiconductor materials, is expected to enable strong many-body interactions like exciton-exciton annihilation (EEA). Several groups have recently demonstrated that monolayer TMDC materials may have EEA rates two orders of magnitude greater than conventional semiconductor materials [6-9]. However, many important questions of the EEA have remained to be answered. There is no quantitative understanding about how much the EEA could affect the light emission properties of the monolayers. And no study is available on how the EEA could depend on the environment at the proximity of the monolayers such as substrates. Additionally, substantial discrepancy can be found in the results of previous studies, as some reported no EEA in the monolayers[10-12] at which strong EEA were observed by others[7,8].

Here we quantitatively elucidate the fundamental limit that the EEA imposes to the luminescence efficiency and lasing threshold in monolayer TMDC materials. We evaluate the EEA rate and its role in light emission for suspended monolayers and the monolayers supported by substrates. The EEA may substantially affect the luminescence efficiency of suspended monolayers even at a photogenerated carrier concentration as low as 10^9 cm^{-2} , while plays a milder role for the supported monolayers owing to the effect of substrates, which may decrease the EEA rate and enables defect-assisted channels to compete with the EEA for the excitons to decay. But

regardless the presence of substrates or not, the lasing threshold of the monolayers is always predominantly determined by the EEA. Our results also suggest that the conflicting results in the previous studies [7,8,10-12] are likely due to the different interactions with substrates.

Fig. 1 shows the PL efficiencies (defined as the number of emitted photons vs. the number of adsorbed photons) of suspended monolayer MoS₂ and WS₂ as a function of incident laser power (see Fig. S1 for the result of WSe₂). The samples were made by manually transferring chemical vapor deposition-grown monolayers onto SiO₂/Si substrates pre-patterned with holes (see Methods and Fig. S2)[13]. The efficiency is evaluated from PL measurements at room temperatures and by using Rhodamine 6G as a reference. The efficiencies vary among these materials with WS₂ showing the highest efficiency followed by WSe₂ and MoS₂, but all exhibit an exponential decrease with the incident power increasing, even at a power as low as 10 W/cm². In stark contrast, the PL efficiencies of as-grown monolayers show much milder dependence on the incident power (Fig. S4). We can exclude out heating effects in the measurement as the temperature change in the monolayers is expected no more than 20°C (see Fig.S3). The negligible heating effect is also supported by a constant lineshape and position of the PL peak through the measurement (Fig. S4), as redshift and broadening of the PL peak would be expected should substantial heat be generated [14-16]. Additionally, the constant PL lineshape and frequency indicate negligible formation of bi-excitons, which would otherwise give rise to a new peak with energy lower than the normal PL peak [17-19]. With the exclusion of heating effect and bi-excitons, the non-linear power-dependence of the PL efficiency strongly suggests the presence of exciton-exciton annihilation (EEA).

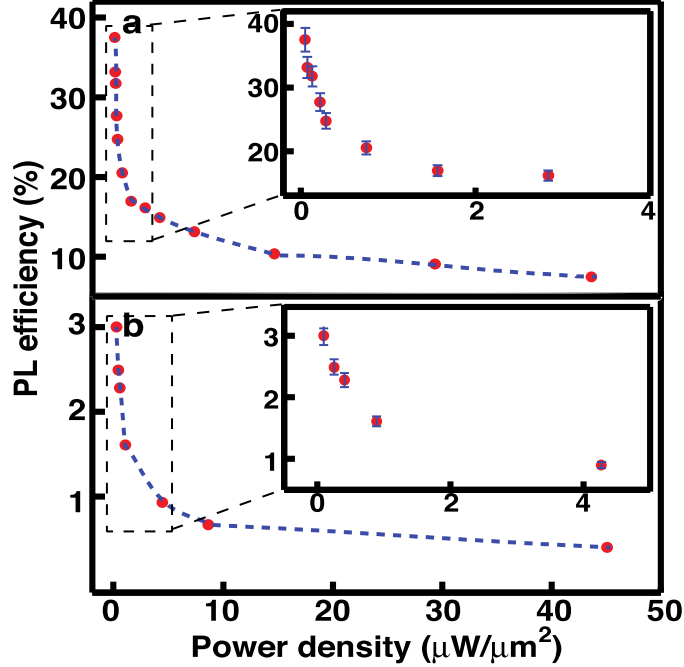


FIG 1. PL efficiencies of (a) suspended monolayer WS₂ and (b) suspended monolayer MoS₂ as a function of the incident power density. The blue dashed lines just serve to guide the vision. The inset is to magnify the results in the corresponding dashed box, error bar: 10%.

To better understand the EEA, we examined the exciton dynamics in the monolayers using pump-probe techniques (see Methods). What we measured is the differential reflection $\Delta R/R$ of a delayed probe beam from the monolayers after photoexcitation by a pump beam (590 nm). The wavelength of the probe beam is chosen to match the A exciton of the monolayer, and the pumping fluence is set to be small enough to ensure the absorption far below being saturated. As a result, the differential reflection ($\Delta R/R$) can be linearly correlated to the concentration of photo-generated charge carriers at the band edges. Fig. 2 shows the transient differential reflection $\Delta R/R$ collected from suspended WS₂ monolayers (see Fig. S5-S7 for more results). We confirmed no substantial heating effect during the experiments by ensuring a linear dependence of the $\Delta R/R$ at the 0s delay ($\Delta R/R$)₀ on the pumping fluence as ($\Delta R/R$)₀ is found dependent on the temperature (Fig. S8). The result in Fig. 2a indicates that the decay rate increases with the

pumping fluence, consistent with what expected from the presence of EEA. The increase of the decay rate also indicates no substantial formation of bi-excitons, which would otherwise slow the decay [19].

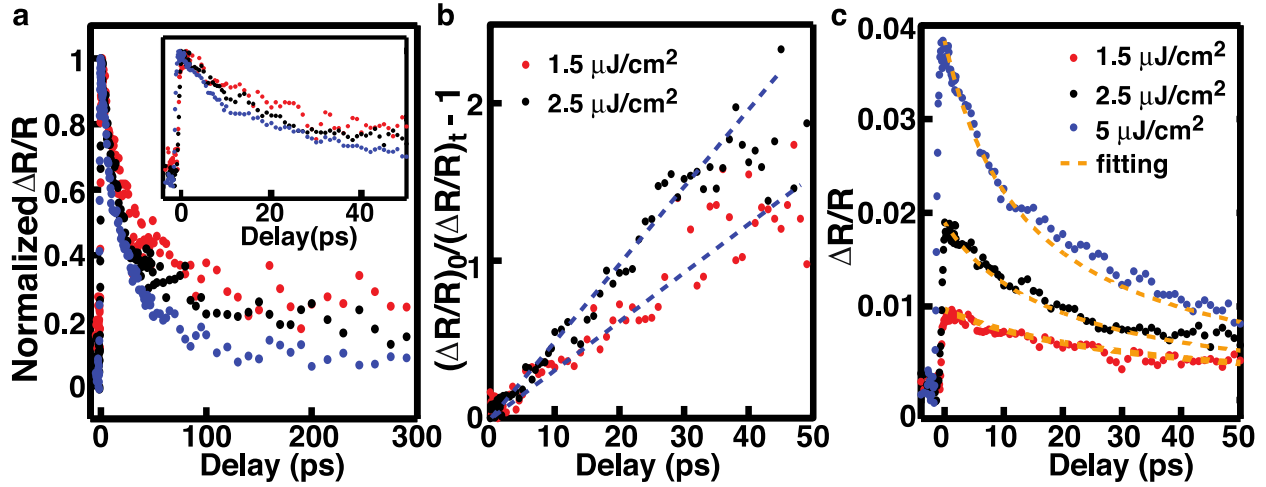


FIG 2. (a) Normalized differential reflection of suspended WS_2 with different pumping fluences, 1.5 $\mu\text{J}/\text{cm}^2$ (red), 2.5 $\mu\text{J}/\text{cm}^2$ (blue), and 5.0 $\mu\text{J}/\text{cm}^2$ (black). Inset: the results for the early stage of the decay. (b) The result of $(\Delta R/R)_0/(\Delta R/R)_t - 1$ derived from the data in (a). The dashed line serves to illustrate the slope of the result. (c) Fitting for the measured differential reflection of suspended WS_2 with different pumping fluences, The fitted results are plotted in dashed lines and the experimental results are dots, 1.5 $\mu\text{J}/\text{cm}^2$ (red), 2.5 $\mu\text{J}/\text{cm}^2$ (blue), and 5.0 $\mu\text{J}/\text{cm}^2$ (black).

We can quantitatively evaluate the rate constant of the EEA based on the dynamic measurement.

For the exciton decay dominated by EEA, the rate equation of exciton density can be written as a function of the EEA rate k_{ee} , $dN/dt = -k_{ee}N^2$. And the exciton density $N(t)$ can be correlated to the total photo-generated excitons N_0 as

$$\frac{N_0}{N(t)} - 1 = k_{ee}N_0t \quad (1)$$

Assuming that each absorbed photon may generate one exciton at the band edge, $(\Delta R/R)_0$ essentially represents the total photo-generated excitons N_0 and we may have $N_0/N(t) = (\Delta R/R)_0/(\Delta R/R)_t$. We can derive $(\Delta R/R)_0/(\Delta R/R)_t - 1$ from the result given in Fig. 2a, and plot it as

a function of the delay time in Fig. 2b. The result shows that $(\Delta R/R)_0/(\Delta R/R)_t - 1$ linearly depends on the delay time at the early stage of the decay (up to 50-100 ps) and its slope linearly increases with the pumping fluence (Fig. 2b). This is consistent with what expected from eq. (1), indicating that the exciton decay in the monolayers is indeed dominated by EEA. The total photo-generated excitons N_0 is related with the absorption efficiency of the monolayers, which is estimated to be 0.058 and 0.022 in suspended WS₂ and MoS₂ using the refractive index of the monolayers we measured (See Ref. 3 and Fig. S9). The rate constant k_{ee} can thus be derived as 0.3 cm²/s and 0.1 cm²/s for suspended WS₂ and MoS₂ monolayers, respectively.

The substrate may have significant effects on the EEA. We performed similar pump-probe measurements and data analysis for the as-grown MoS₂ and WS₂ monolayers onto sapphire substrates (Fig.S6-S7). The EEA rate of the supported monolayer is found smaller than that of the suspended counterpart, 0.1 cm²/s and 0.05 cm²/s for the supported WS₂ and MoS₂, respectively. The result for supported MoS₂ monolayers is reasonably consistent with what previously reported (0.04 cm²/s)[8]. The smaller EEA rate of the supported monolayers indicates the substantial effect of the substrate and can be understood from an intuitive perspective. Generally, the rate of EEA is related with the diffusion coefficient of excitons D and the annihilation radius R that represents the separation of two excitons when the annihilation may occur, $k_{ee} = 4\pi DR$ [20]. The presence of the substrate may lower the mobility of charges [21] as well as the exciton binding energy[22,23], the latter of which could subsequently lead to a smaller R . Besides from lowering the EEA rate, the substrate may also affect the EEA by enabling defect-assisted decay of excitons [11,24]. While the defect-assisted decay may not change the EEA rate, it could make the observation of the EEA more difficult when the defect-

assisted decay rate is comparable to or faster than the EEA rate. For instance, the EEA in the supported MoS₂ can be observed only in the first several ps (< 2 ps) and by using relatively high pumping fluence (> 25 μJ/cm²) (Fig.S7). We found in experiments that generally it was more difficult to observe the EEA in the monolayers showing lower PL intensities and faster exciton decay due to stronger interactions with the substrate. Given the significant effect of substrates on the EEA, we believe that the discrepancies in the previous studies, i.e., the demonstration of different EEA rates in the same materials by different groups [7,8,10-12], is likely due to different interactions of the monolayer with substrates.

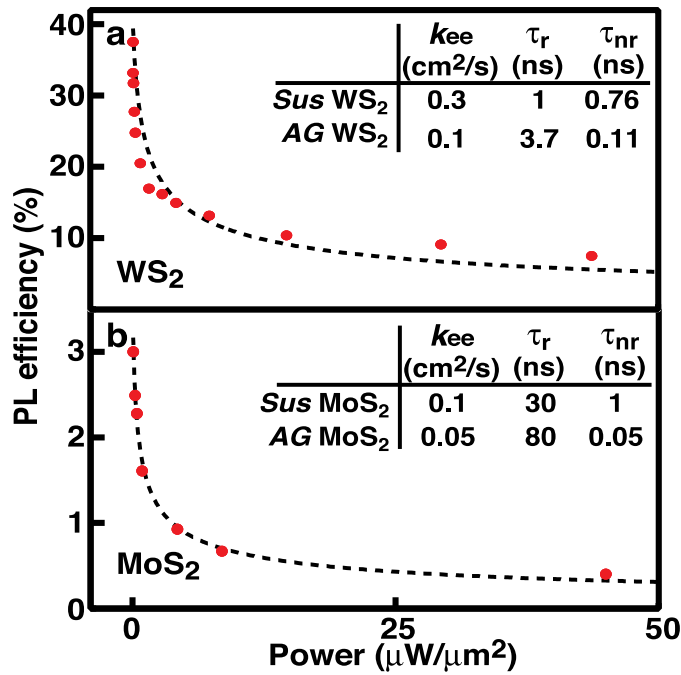


FIG. 3. Fitting for the measured power-dependent PL efficiencies of (a) suspended monolayers WS₂ and (b) suspended monolayer MoS₂. The fitted results are plotted in dashed lines and the experimental results are dots. The inset shows the fitted parameters for suspended (Sus) and as-grown (AG) monolayers. The fitting for the as-grown monolayers is given in Fig. S10.

We can obtain useful insight into the power-dependent luminescence efficiency (Fig.1) by correlating the efficiency to the nonlinear and linear decay processes involved. The rate equation of exciton density for the time-averaged PL can be written as

$$\frac{dN}{dt} = -\left(\frac{1}{\tau_r} + \frac{1}{\tau_{nr}}\right)N - k_{ee}N^2 + \alpha I_0 \quad (2)$$

where τ_r and τ_{nr} represent the exciton lifetimes associated with radiative and linear non-radiative recombinations, α and I_0 are the absorption efficiency for the incident wavelength and the incident power density, respectively. From eq. (2) we can derive the PL efficiency (quantum yield) at steady state ($dN/dt = 0$) as

$$QY = \frac{N / \tau_r}{\alpha I_0} = \frac{\left[\sqrt{(1 / \tau_r + 1 / \tau_{nr})^2 + 4 k_{ee} \alpha I_0} - (1 / \tau_r + 1 / \tau_{nr}) \right]}{2 k_{ee} \alpha I_0 \tau_r} \quad (3)$$

The absorption efficiency α of suspended monolayer MoS₂ and WS₂ is calculated to be 0.065 and 0.055, respectively, for the incident laser (532 nm) using the refractive index of the monolayers we measured (See Ref. 3 and Fig. S9). With the EEA rate k_{ee} obtained from the dynamics measurement, we can evaluate τ_r and τ_{nr} by numerically fitting the measured power-dependent efficiency to eq. (3). Fig. 3 shows the fitting results and the fitted value of τ_r and τ_{nr} for suspended monolayer MoS₂ and WS₂. We may find the value of τ_r and τ_{nr} for supported monolayers by performing similar fittings (Fig. S10).

Knowledge for the EEA and the lifetimes of linear decay processes may provide guidance for the design of light emission devices. It helps determine the proper density of injected charges for the realization of high quantum yield in light emission devices. According to eq. (2), EEA may turn to be the major pathway for the exciton to decay when the exciton density $N > (k_r + k_{nr})/k_{ee}$, which can be in the scale of 10^{10} cm^{-2} and 10^{11} cm^{-2} for suspended and supported monolayers,

respectively. The density of injected charges must be well below this value in order to minimize the adverse effect of the EEA. This notion can be more clear illustrated by Fig. S11, in which the result of Fig. 1 is re-plot as a function of the carrier concentration that we evaluate using eq. (3). More importantly, knowledge for the EEA and the lifetimes may help predict the lasing threshold and optical gain coefficient. We use a simple three-level system to represent the pumping process in the monolayer (Fig.4a inset), in which the charges at the ground state 1 (valence band edge) are first pumped to the upper pump level 3 (a higher level in the conduction band) and then quickly decay to the level 2 (the edge of the conduction band). The intraband decay from the level 3 to the level 2 is very fast, in scale of < 1 ps [25], and the population of the charge carriers at the level 3 can thus be ignored.

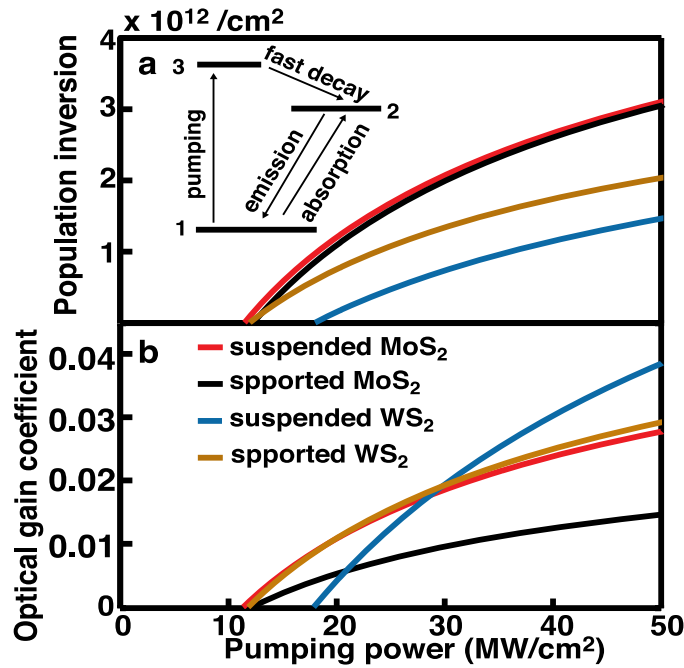


FIG. 4. (a) Calculated population inversion and (b) optical gain coefficients for different monolayers, including suspended monolayer MoS_2 (red), supported MoS_2 (black), suspended WS_2 (blue), and supported WS_2 (brown). Inset, a schematic illustration of the three-level model used for the calculation.

The rate equation for the charge density at the level 2 can be written as

$$\frac{dN_2}{dt} = -\sigma_{12} \frac{I}{h\nu_{12}} (N_2 - N_1) - \left(\frac{1}{\tau_r} + \frac{1}{\tau_{nr}}\right) N_2 - k_{ee} N_2^2 + \sigma_{13} \frac{I_p}{h\nu_{13}} N_1 \quad (4)$$

where σ_{12} is the stimulated emission (absorption) cross section for the light in frequency ν_{12} that matches the energy difference between the level 1 and level 2, I is the photon flux at the frequency of ν_{12} , h is the Planck's constant, σ_{13} is the absorption cross section for the pumping light in frequency ν_{13} , and I_p is the pumping intensity. By using the steady state ($dN_2/dt = 0$) and the conservation of charges ($N_2 + N_1 = N_t$, N_t is the total charge density), we can find out the population inversion ($N_2 - N_1$) as

$$\Delta N = N_2 - N_1 = \frac{\sqrt{\left(1/\tau_r + 1/\tau_{nr} + W_p\right)^2 + 4k_{ee}W_pN_t} - \left(1/\tau_r + 1/\tau_{nr} + W_p\right) - k_{ee}N_t}{k_{ee}} \quad (5)$$

and the optical gain coefficient as $\gamma = \sigma_{12} \Delta N$, where $W_p = \sigma_{13} I_p / h\nu_{13}$ representing the pumping rate. In the process of deriving eq. (5) we assume a small-signal inversion ($I \ll I_p$) and ignore the term of $\sigma_{12} I / h\nu_{12}$. According to eq. (5), to achieve population inversion ($\Delta N > 0$) requires $W_p > k_{ee} N_t / 2 + (1/\tau_r + 1/\tau_{nr})$, i.e. the pumping rate being larger than the decay rate.

The EEA plays a dominant role in determining the lasing threshold and optical gain of the monolayers. The total charge density N_t of monolayer WS₂ and MoS₂ can be estimated to be $4.17 \times 10^{12} \text{ cm}^{-2}$ and $6.27 \times 10^{12} \text{ cm}^{-2}$, respectively, by assuming parabolic band edges at K point and using the average effective mass reported in the literature ($0.4m_0$ and $0.6m_0$ for WS₂ and MoS₂) [26-29]. Based on the value given in Fig. 3, $k_{ee} N_t / 2$ is always one or two orders of magnitude larger than $1/\tau_r + 1/\tau_{nr}$ for all the supported and suspended monolayers. As a result, essentially the threshold pumping rate $W_p = k_{ee} N_t / 2$ as $k_{ee} N_t / 2 \gg 1/\tau_r + 1/\tau_{nr}$. And the population inversion can be simplified as $\Delta N = \left(\sqrt{W_p^2 + 4k_{ee}W_pN_t} - W_p\right) / k_{ee} - N_t$. Without losing generality,

we use the pumping wavelength of 532 nm as an example to numerically evaluate the population inversion and optical gain coefficient on the pumping intensity I_p . The stimulated emission (absorption) cross section σ_{13} (or σ_{12}) can be derived from the total charge density and the absorption efficiency α_{13} (or α_{12}), the latter of which can be calculated using the dielectric function of the monolayers (See Ref. 3 and Fig. S9), $\sigma_{13} = \alpha_{13}/N_t$. Fig. 4 shows the calculated population inversion and optical gain coefficient as a function of pumping power (532 nm). The threshold pumping power for population inversion is around 18 MW/cm² for suspended monolayer WS₂ and around 12 MW/cm² for all the other monolayers. This calculation neither take into account any optical enhancement effects, heating effect during the pumping, nor any possible re-normalization of the bandgap [23,30]. It nevertheless provides useful guidance for the development of 2D TMDC lasers operated at room temperatures. This predicted threshold pumping power is reasonably consistent with one recent study, in which the threshold pumping power for lasing in supported WS₂ monolayer is estimated at 5-8 MW/cm² [31].

In conclusion, we have quantitatively evaluated the exciton-exciton annihilation (EEA) in monolayer TMDC materials and its effect on the monolayers' light emission properties, including luminescence efficiency and lasing threshold. We also show that the EEA rate is dependent on the interaction of the monolayer with substrates, which could be the reason for the discrepancy in previous studies. The result may provide useful guidance for the rational design of atomic-scale light emission devices, including LEDs and lasers.

[1] L. Y. Cao, *Nature* **40**, 592 (2015).

- [2] K. L. He, N. Kumar, L. Zhao, Z. F. Wang, K. F. Mak, H. Zhao, and J. Shan, *Phys Rev Lett* **113** (2014).
- [3] Y. Yu *et al.*, *Sci. Rep.* **5**, 16996 (2015).
- [4] H. M. Hill, A. F. Rigosi, C. Roquelet, A. Chernikov, T. C. Berkelbach, D. R. Reichman, M. S. Hybertsen, L. E. Brus, and T. F. Heinz, *Nano Lett*, DOI: 10.1021/nl504868p (2015).
- [5] B. Zhu, X. Chen, and X. Cui, *Sci. Rep.* **5**, 9218 (2014).
- [6] N. Kumar, Q. N. Cui, F. Ceballos, D. W. He, Y. S. Wang, and H. Zhao, *Phys Rev B* **89** (2014).
- [7] S. Mouri, Y. Miyauchi, M. Toh, W. J. Zhao, G. Eda, and K. Matsuda, *Phys Rev B* **90** (2014).
- [8] D. Z. Sun, Y. Rao, G. A. Reider, G. G. Chen, Y. M. You, L. Brezin, A. R. Harutyunyan, and T. F. Heinz, *Nano Lett* **14**, 5625 (2014).
- [9] L. Yuan and L. B. Huang, *Nanoscale* **7**, 7402 (2015).
- [10] H. Shi, R. Yan, S. Bertolazzi, J. Brivio, B. Gao, A. Kis, D. Jena, H. G. Xing, and L. Huang, *ACS Nano* **7**, 1072 (2013).
- [11] H. N. Wang, C. J. Zhang, and F. Rana, *Nano Lett* **15**, 339 (2015).
- [12] Q. Cui, F. Ceballos, N. Kumar, and H. Zhao, *ACS Nano* **8**, 2970 (2014).
- [13] A. Gurarlsan *et al.*, *ACS Nano* **11**, 11522 (2014).
- [14] T. Korn, S. Heydrich, M. Hirmer, J. Schmutzler, and C. Schuller, *Appl Phys Lett* **99** (2011).
- [15] S. Tongay, J. Zhou, C. Ataca, K. Lo, T. S. Matthews, J. B. Li, J. C. Grossman, and J. Q. Wu, *Nano Lett* **12**, 5576 (2012).
- [16] L. Q. Su, Y. F. Yu, L. Y. Cao, and Y. Zhang, *Nano Res* **8**, 2686 (2015).

- [17] G. Plechinger, P. Nagler, J. Kraus, N. Paradiso, C. Strunk, C. Schuller, and T. Korn, *Phys Status Solidi-R* **9**, 457 (2015).
- [18] E. J. Sie, A. J. Frenzel, Y. H. Lee, J. Kong, and N. Gedik, *Phys Rev B* **92** (2015).
- [19] Y. M. You, X. X. Zhang, T. C. Berkelbach, M. S. Hybertsen, D. R. Reichman, and T. F. Heinz, *Nat Phys* **11**, 477 (2015).
- [20] G. M. Akselrod, Y. R. Tischler, E. R. Young, D. G. Nocera, and V. Bulovic, *Phys. Rev. B* **82**, 113106 (2010).
- [21] N. Ma and D. Jena, *Phys. Rev. X* **4**, 011043 (2014).
- [22] Y. X. Lin, X. Ling, L. L. Yu, S. X. Huang, A. L. Hsu, Y. H. Lee, J. Kong, M. S. Dressehaus, and T. Palacios, *Nano Lett* **14**, 5569 (2014).
- [23] M. M. Ugeda *et al.*, *Nat Mater* **13**, 1091 (2014).
- [24] C. J. Docherty, P. Parkinson, H. J. Joyce, M.-H. Chiu, C.-H. Chen, M.-Y. Lee, L.-J. Li, L. M. Herz, and M. B. Johnston, *ACS Nano* **8**, 11147 (2014).
- [25] Z. G. Nie *et al.*, *Acs Nano* **8**, 10931 (2014).
- [26] W. S. Yun, S. W. Han, S. C. Hong, I. G. Kim, and J. D. Lee, *Phys Rev B* **85** (2012).
- [27] T. Cheiwchanchamnangij and W. R. L. Lambrecht, *Phys Rev B* **85** (2012).
- [28] H. Peelaers and C. G. Van de Walle, *Phys Rev B* **86** (2012).
- [29] H. L. Shi, H. Pan, Y. W. Zhang, and B. I. Yakobson, *Phys Rev B* **87** (2013).
- [30] A. Chernikov, C. Ruppert, H. M. Hill, A. F. Rigosi, and T. F. Heinz, *Nat. Photon.* **9**, 466 (2015).
- [31] Y. Ye, Z. J. Wong, X. Lu, X. Ni, H. Zhu, X. Chen, Y. Wang, and X. Zhang, *Nat. Photon.* **9**, 733 (2015).

Supplementary Information

**Limits of Exciton-Exciton Annihilation for Light Emission in Transition
Metal Dichalcogenide Monolayers**

Yiling Yu^{1,2§}, Yifei Yu^{1§}, Chao Xu^{2§}, Andy Barrette², Kenan Gundogdu^{2*}, Linyou Cao^{1,2*}

¹Department of Materials Science and Engineering, North Carolina State University, Raleigh NC 27695;

²Department of Physics, North Carolina State University, Raleigh NC 27695;

§ These authors contribute equally.

* To whom correspondence should be addressed.

Email: lcao2@ncsu.edu, kgundog@ncsu.edu

This PDF document includes

Methods

Figure S1-S11

References

Methods

Synthesis and transfer of MoS₂, WS₂, and WSe₂ monolayers: The monolayers were grown using a chemical vapor deposition (CVD) reported previously¹. Typically, 1g sulfur or selenium powder (Sigma-Aldrich) and 15-30mg MoO₃ (WO₃) (99.99%, Sigma-Aldrich) source material were placed in the upstream and the center of a tube furnace, respectively. And substrates (usually sapphire) were placed at the downstream of the tube. Typical growth was performed at 750-900 °C) for 10 (30) minutes under a flow of Ar gas in rate of 100 sccm and ambient pressure.

The transfer of the monolayers followed a surface-energy-assisted transfer approach that we have developed previously². In a typical transfer process, 9 g of polystyrene (PS) with a molecular weight of 280000 g/mol was dissolved in 100 mL of toluene, and then the PS solution was spin-coated (3000 rpm for 60 s) on the as-grown monolayers. This was followed by a baking at 80–90 °C for 1 hour. A water droplet was then dropped on top of the monolayer. Due to the different surface energies of the monolayer and the substrate, water molecules could penetrate under the monolayer, resulting the delamination of the PS-monolayer assembly. We could pick up the polymer/monolayer assembly with a tweezers and transferred it to different substrates. After that, we baked the transferred PS-monolayer assembly at 80 °C for 1 h and performed a final baking for 30 min at 150 °C. Finally, PS was removed by rinsing with toluene several times.

Characterizations: Raman and AFM measurements were used to confirm that the synthesized samples are monolayers. The Raman measurements were carried out by Horiba Labram HR800 system with a 532 nm laser. AFM measurements were performed at a Veeco Dimension-3000 atomic force microscope. A home-built setup that consists of a confocal microscope (Nikon Eclipse C1) connected with a monochromator (SpectraPro, Princeton Instruments) and a detector (Pixis, Princeton Instruments) was used to perform the photoluminescence measurement with an excitation wavelength of 532nm.

A 150 fs pulse at 2.10 eV is used to pump electrons from the valence band into conduction band of the monolayers. The differential reflection ($\Delta R/R$) of a time-delayed probe pulse, whose wavelength is chosen to match the A exciton transition (~ 1.88 eV for MoS₂ and 2eV for WS₂, respectively), was used to probe the excitation dynamics. The pump and probe beams were collinearly polarized and co-focused using a 50X long working distance objective and the reflected probe pulse was collected using the same objective. The size of the focused beam is about 2 μ m. A monochromator and a Si photodetector combination measure the differential reflection using lock-in amplification method. Unless otherwise specified, all experiments were performed at room temperature.

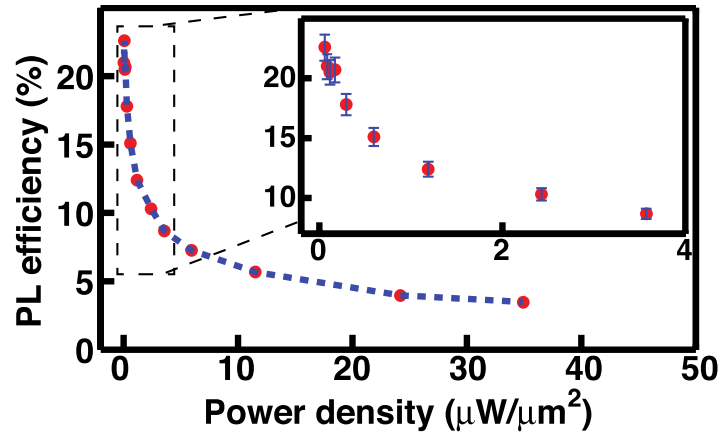


Figure S1. Photoluminescence efficiency of suspended monolayer WSe₂ as a function of incident power density (wavelength 532 nm). The dashed line serves to guide the vision. The inset is a magnified version for the results in the dashed box. For visual convenience, the error bar (5%) are only added in the figure in the inset.

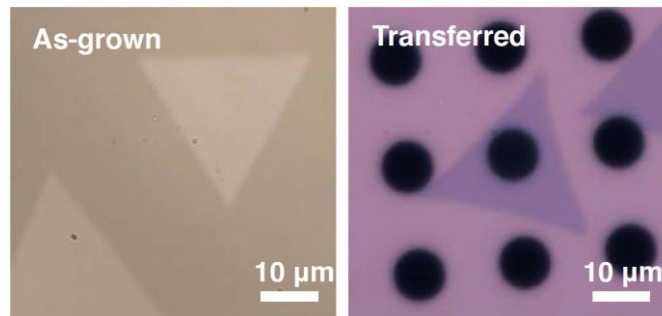


Figure S2. Optical image of typical as-grown monolayers on sapphire substrates and transferred monolayers on SiO₂/Si substrates pre-patterned with holes. The black areas are the pre-patterned holes on the substrate.

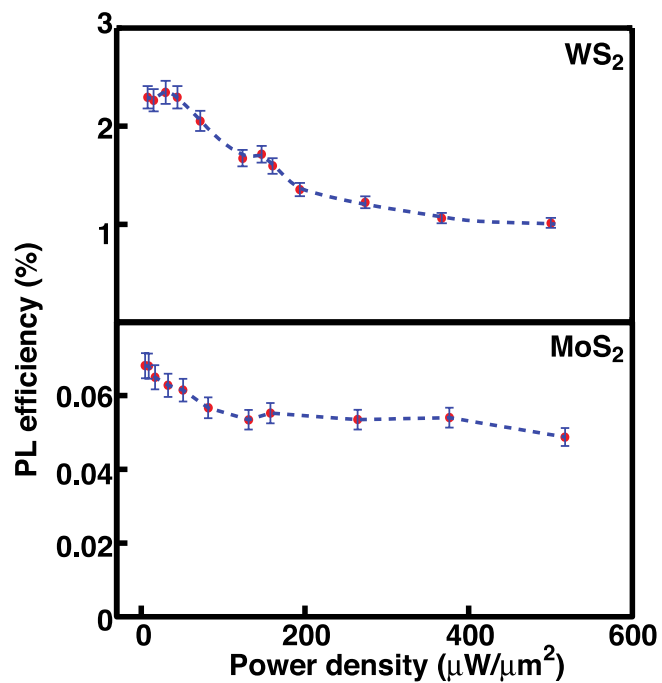


Figure S3. Photoluminescence efficiency of as-grown monolayer WS₂ on sapphire substrates (upper) and as-grown monolayer MoS₂ on sapphire substrates as a function of incident power density (wavelength 532 nm). The dashed line serves to guide the vision.

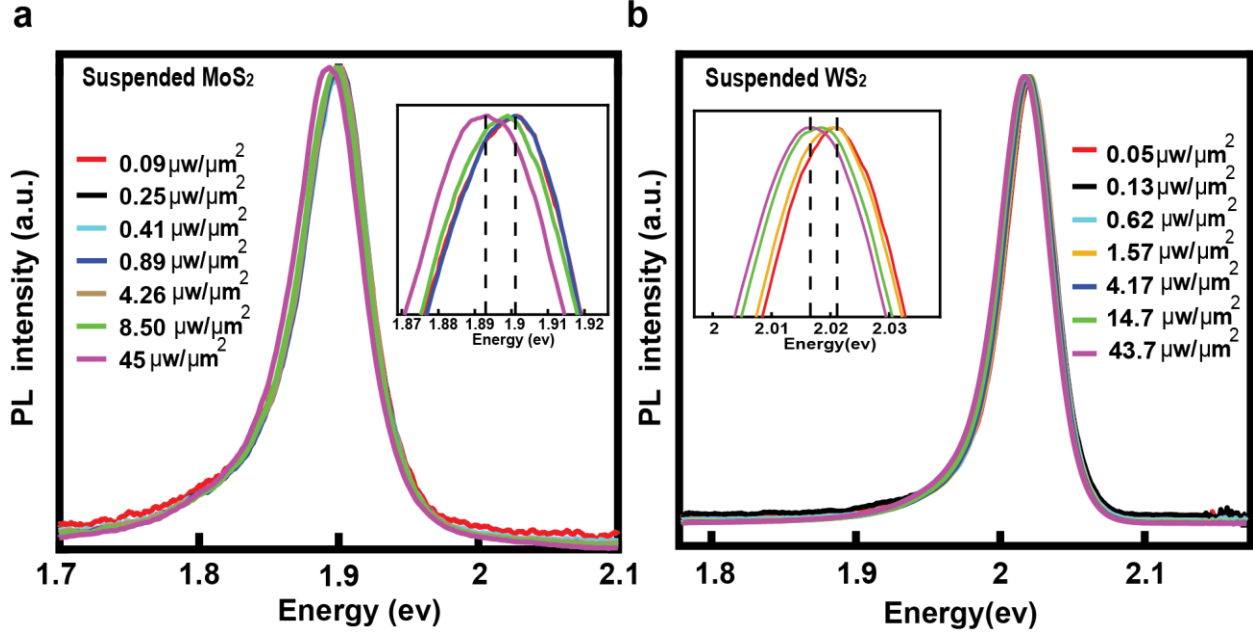


Figure S4. Dependence of the PL spectra of suspended MoS₂ and WS₂ on incident power. (a) PL spectra of suspended MoS₂ at different incident powers. Inset: Zoom-in curves of 4 representative powers, the black dash lines denotes PL peak position at the lowest and highest incident powers used in the experiments. The temperature change in the sample can be estimated by this peak shift (~ 8 meV) using the well-established temperature dependent band-gap equation $E_g(T) = E_g(0) - \alpha T^2 / (T + \beta)$ and $\alpha = 5.9 \times 10^{-4} \text{ eV/K}$, $\beta = 430 \text{ K}$ from Ref.S3, the temperature change is calculated to be around 20K with the incident power $50 \mu\text{W}/\text{cm}^2$. (b) PL spectra of suspended WS₂ at different incident powers. Similar to suspended MoS₂, the peak shift is small and there is essentially no change in the PL lineshape.

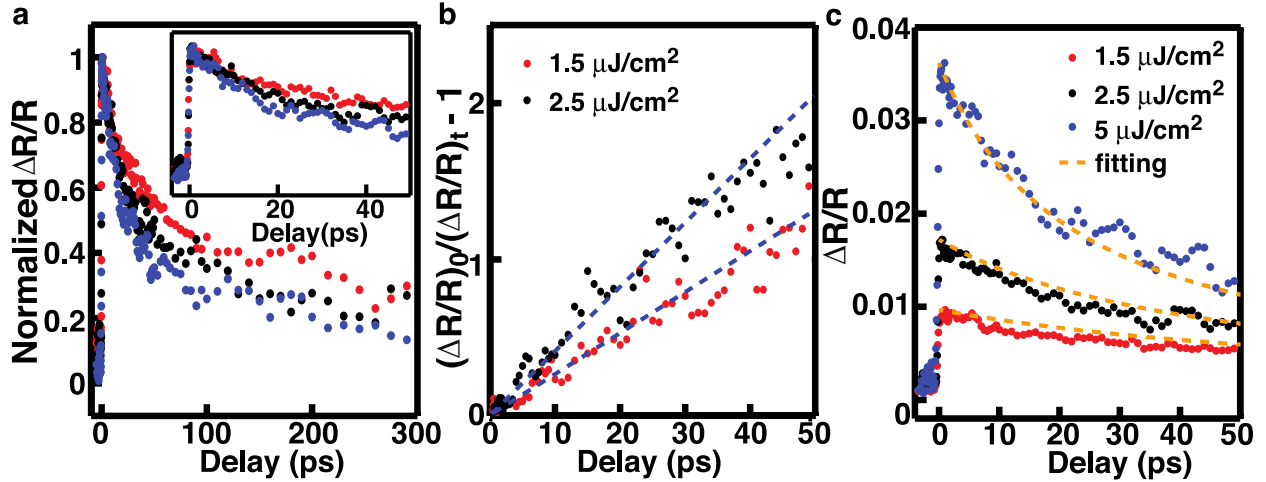


Figure S5. (a) Normalized differential reflection of suspended MoS_2 as a function of the time delay and with different pumping fluences, 1.5 $\mu\text{J}/\text{cm}^2$ (red), 2.5 $\mu\text{J}/\text{cm}^2$ (black), and 5.0 $\mu\text{J}/\text{cm}^2$ (blue). Inset: the results for the early stage of the decay. (b) The result of $(\Delta R/R)_0/(\Delta R/R)_t - 1$ derived from the data in (a) as a function of the delay time. The result for the pumping fluence of 5.0 $\mu\text{J}/\text{cm}^2$ is not shown for the visual convenience. (c) Fitting for the measured differential reflection of suspended MoS_2 with different pumping fluences, The fitted results are plotted in dashed lines and the experimental results are dots, 1.5 $\mu\text{J}/\text{cm}^2$ (red), 2.5 $\mu\text{J}/\text{cm}^2$ (black), and 5.0 $\mu\text{J}/\text{cm}^2$ (blue).

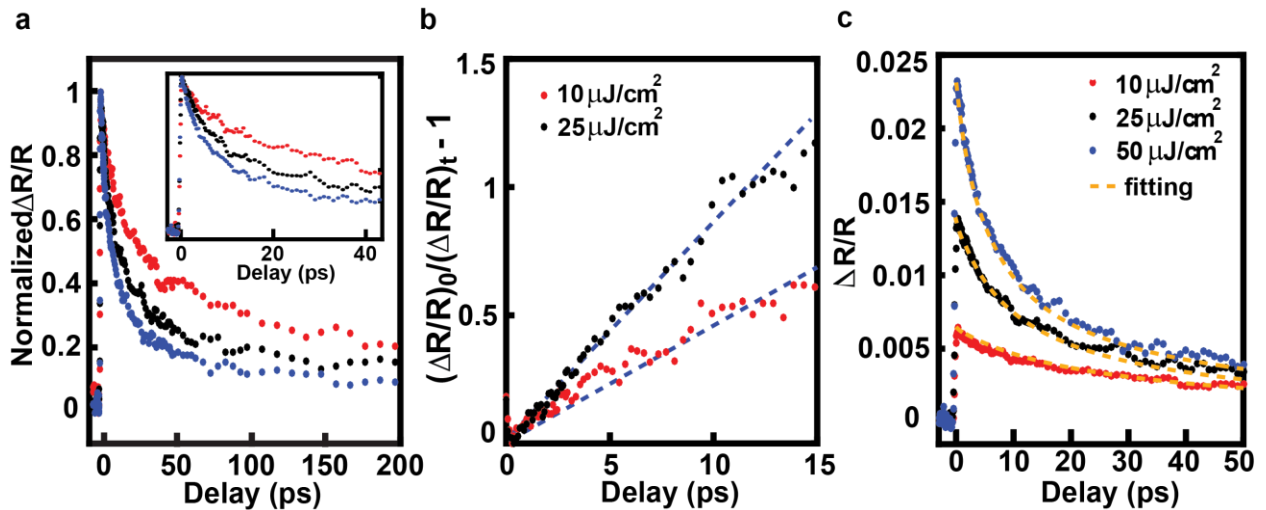


Figure S6. (a) Normalized differential reflection of as-grown WS_2 as a function of the time delay and with different pumping fluences, 10 $\mu\text{J}/\text{cm}^2$ (red), 25 $\mu\text{J}/\text{cm}^2$ (black), and 50 $\mu\text{J}/\text{cm}^2$ (blue). Inset: the results for the early stage of the decay. (b) The result of $(\Delta R/R)_0/(\Delta R/R)_t - 1$ derived from the data in (a) as a function of the delay time. The result for the pumping fluence of 50 $\mu\text{J}/\text{cm}^2$ is not shown for the visual convenience. (c) Fitting for the measured differential reflection of as grown WS_2 with different pumping fluences, The fitted results are plotted in dashed lines and the experimental results are dots, 10 $\mu\text{J}/\text{cm}^2$ (red), 25 $\mu\text{J}/\text{cm}^2$ (black), and 50 $\mu\text{J}/\text{cm}^2$ (blue).

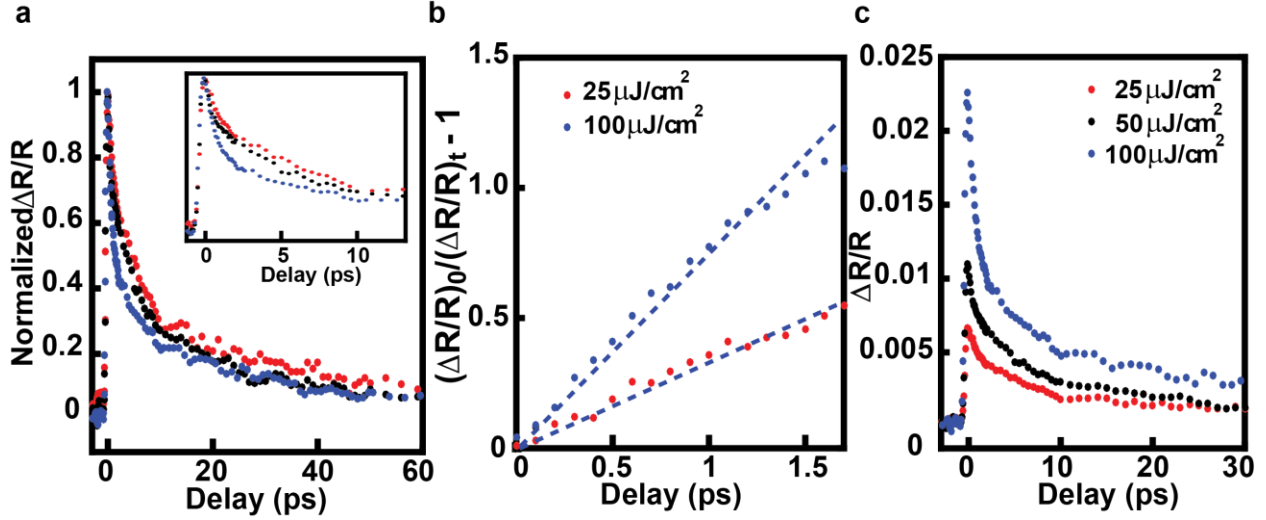


Figure S7. (a) Normalized differential reflection of as-grown MoS₂ as a function of the time delay and with different pumping fluences, 25 $\mu\text{J}/\text{cm}^2$ (red), 50 $\mu\text{J}/\text{cm}^2$ (black), and 100 $\mu\text{J}/\text{cm}^2$ (blue). Inset: the results for the early stage of the decay. (b) The result of $(\Delta R/R)_0/(\Delta R/R)_t - 1$ derived from the data in (a) as a function of the delay time. The result for the pumping fluence of 100 $\mu\text{J}/\text{cm}^2$ is not shown for the visual convenience. (c) The non-normalized differential reflection of as-grown MoS₂ at pumping fluence 25 $\mu\text{J}/\text{cm}^2$ (red), 50 $\mu\text{J}/\text{cm}^2$ (black), and 100 $\mu\text{J}/\text{cm}^2$ (blue).

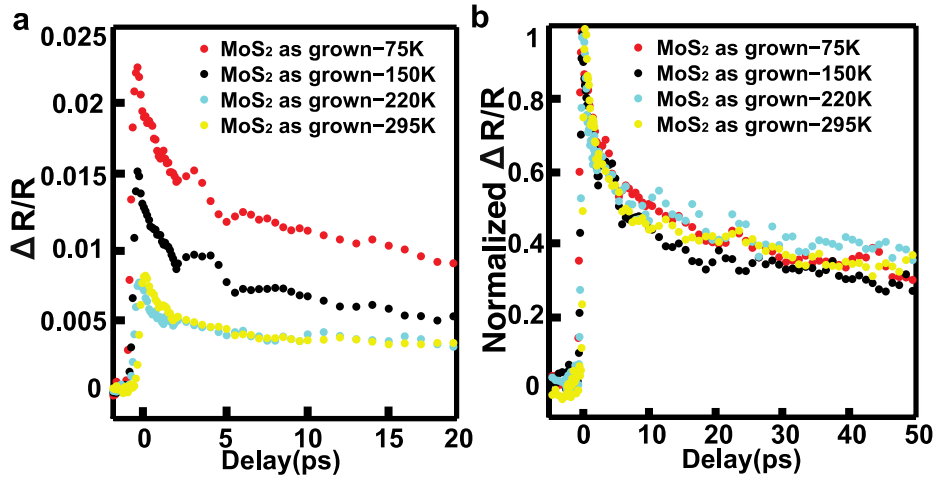


Figure S8. (a) Transient reflection $\Delta R/R$ and (b) normalized $\Delta R/R$ measured at the supported monolayer MoS₂ on sapphire substrates at different temperatures, 75K, 150K, 220K, and 295K. The $\Delta R/R$ at the 0s delay exhibits a strong dependence on the temperature.

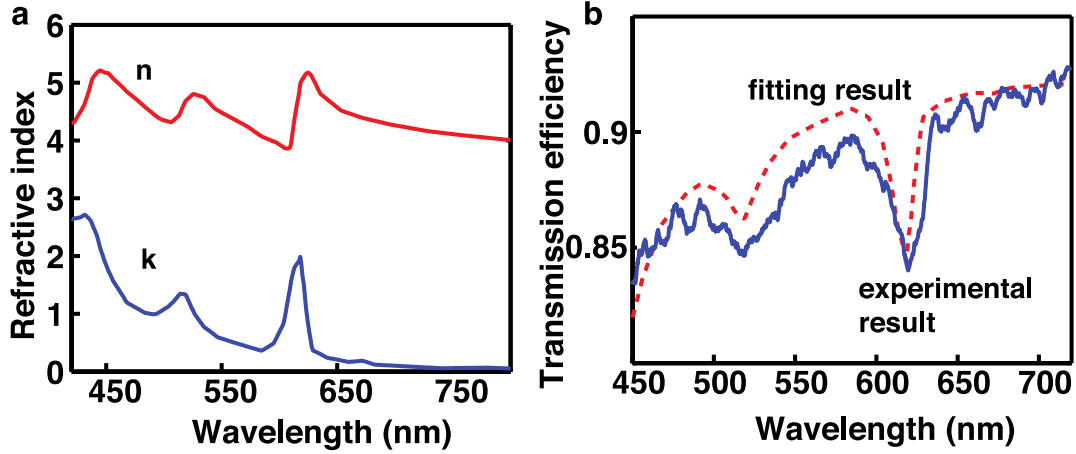


Figure S9. Measured refractive index of monolayer WS₂. (a) measured real and imaginary part of the refractive index of monolayer WS₂. (b) measured and fitted transmission of as-grown monolayer WS₂ on sapphire substrates. The fitting results uses the refractive index given in (a).

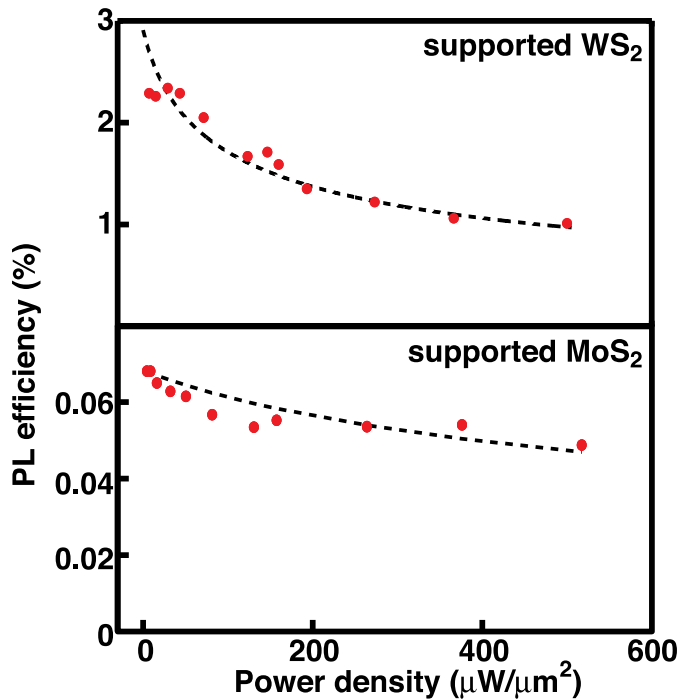


Figure S10. Fitting for the measured power-dependent PL efficiencies of as-grown monolayer WS₂ on sapphire substrates (upper) and as-grown monolayer MoS₂ on sapphire substrates. The fitted results are plotted in dashed lines and the experimental results are dots.

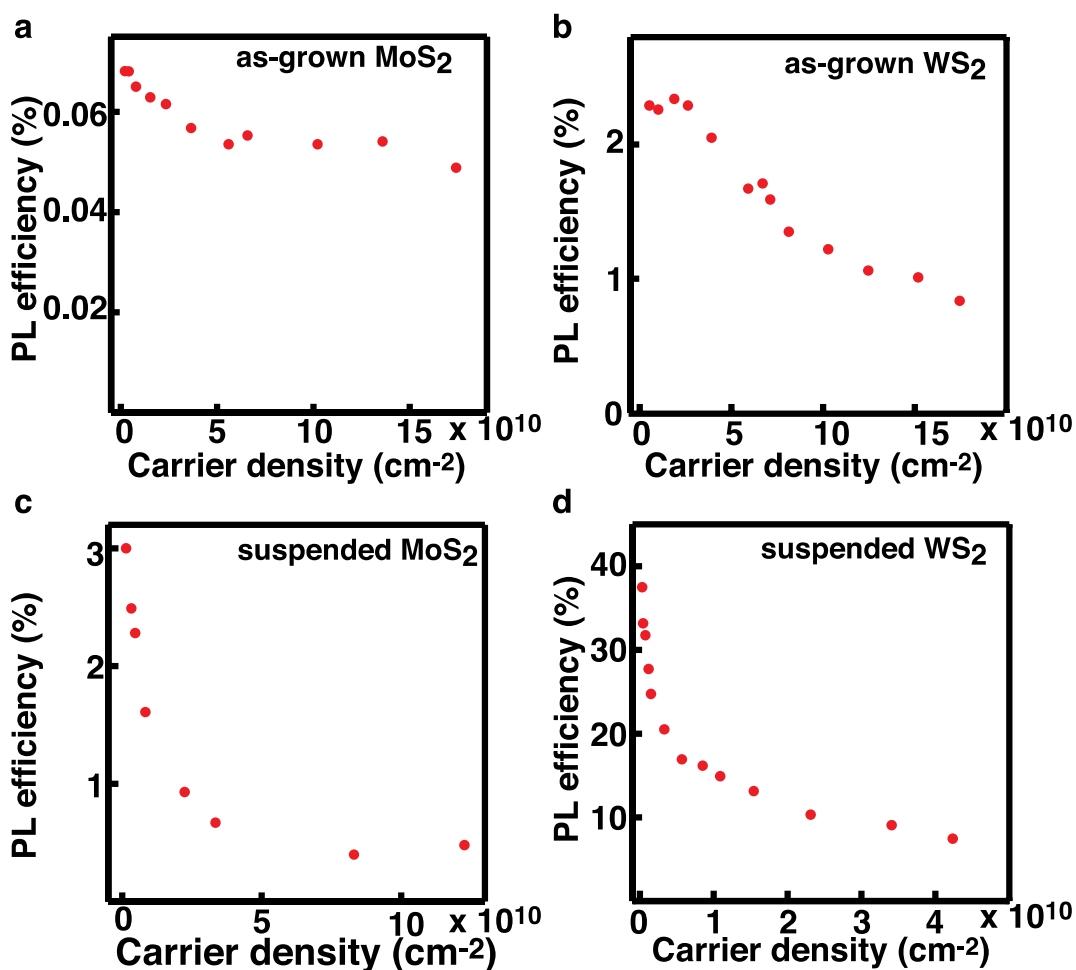


Figure S11. PL efficiencies as a function of the photo-excited carrier density for (a) as-grown monolayer MoS₂ on sapphire substrates, (b) as-grown monolayer WS₂ on sapphire substrates (upper), (c) suspended monolayer MoS₂, and (d) suspended monolayer WS₂.

References

- S1. Yu, Y.; Hu, S.; Su, L.; Huang, L.; Liu, Y.; Jin, Z.; Puzosky, A. A.; Geoghegan, D. B.; Kim, K. W.; Zhang, Y., Equally Efficient Interlayer Exciton Relaxation and Improved Absorption in Epitaxial and Nonepitaxial MoS₂/WS₂ Heterostructures. *Nano Lett* **2014**, *15* (1), 486-491.
- S2. Gurarlan, A.; Yu, Y.; Su, L.; Yu, Y.; Suarez, F.; Yao, S.; Zhu, Y.; Ozturk, M.; Zhang, Y.; Cao, L., Surface-Energy-Assisted Perfect Transfer of Centimeter-Scale Monolayer and Few-Layer MoS₂ Films onto Arbitrary Substrates. *ACS Nano* **2014**, *11*, 11522-11528.
- S3. Korn, T.; Heydrich, S.; Hirmer, M.; Schmutzler, J.; Schuller, C., Low-temperature photocarrier dynamics in monolayer MoS₂. *Appl. Phys. Lett.* **2011**, *99*, 102109.